Adversarially Informed Neural Fields for Computed Tomography Reconstruction

Rasmus Juul Pedersen[1[0009−0007−8395−4270]], Luke Besley[2[0009−0003−1010−6239]], Jakob Sauer Jørgensen[1[0000−0001−9114−754X]], Jens Wenzel Andreasen[2[0000−0002−3145−0229]], Anders Bjorholm Dahl[1[0000−0002−0068−8170]], and Vedrana Andersen Dahl[1[0000−0001−6734−5570]]

[1] Technical University of Denmark, Department of Applied Mathematics and Computer Science
[2] Technical University of Denmark, Department of Energy Conversion and Storage
{rjupe,lubs,jakj,jewa,abda,vand}@dtu.dk

Abstract. We present an adversarially informed neural field (AI-NF) framework for tomographic reconstruction from a limited set of projections—a scenario common in medical imaging, materials science, and other applications where full-angle scans are impractical. Limited projection data renders the reconstruction problem severely ill-posed, often leading to ambiguous and noisy solutions requiring appropriately strong regularization. To address these challenges, our method leverages a continuous neural field representation of the attenuation volume, augmented with data-driven regularization through adversarial learning. Specifically, we integrate an adversarial loss and feature matching into a multilayer perceptron architecture with hash encoding, guiding the reconstruction process by learning complex structural priors from a dataset of high-quality volumes. In our ray-based formulation, the neural attenuation field is integrated along discrete sampling points to simulate projection data, while additional regularization terms (smoothness, consistency, and curvature losses) further stabilize the reconstruction. Experiments on human organs from the Medical segmentation decathlon dataset demonstrate that our approach performs comparably to established methods such as SIRT under noise-free conditions, and it significantly outperforms both traditional iterative and baseline neural field methods in the presence of sinogram noise. Our results highlight the potential of adversarially informed regularization to enhance reconstruction fidelity from sparse and noisy measurements, paving the way for more robust imaging in resource-constrained scenarios. Code available at https://github.com/RasmusJuul/CT-Reconstruction-Neural-Representation

Keywords: CT · · Implicit Neural Representation · Generative adversarial networks (GANs) · Sparse View

1 Introduction

[19] We address the problem of reconstructing a tomographic volume from a limited set of projections, a scenario that arises in medical imaging, materi-

als science, and other fields where full-angle or high-resolution scans may be impractical due to constraints such as radiation exposure, acquisition time, or hardware limitations. This is a severely ill-posed inverse problem, meaning that many different volumes could explain the same limited projection data, leading to ambiguities and loss of detail in the reconstruction.

Regularization is essential for solving ill-posed problems because it imposes constraints and incorporates prior knowledge to reduce ambiguity, suppress noise, and ensure a stable and meaningful solution. Traditional methods use model-based regularization to enforce smoothness or other prior assumptions about the data, but these handcrafted constraints may not fully capture the complex structures present in real-world volumes.

We propose to add data-driven regularization to tomographic reconstruction. Specifically, we use a dataset of previously reconstructed volumes that share similar structural properties with the target volume being reconstructed. Unlike model-based regularization, data-driven approaches allow the reconstruction process to learn complex patterns and correlations directly from real examples.

Our method may be beneficial in scenarios where high-quality volumetric reconstructions of similar objects are available, but new scans must be performed under restrictive conditions—such as minimizing radiation exposure in medical imaging, reducing scan time in industrial applications, or addressing hardware limitations in resource-constrained settings. By incorporating prior knowledge from existing volumes, our approach enables more accurate and robust reconstructions, even when the available projection data is sparse or incomplete.

1.1 Related Work

The standard method in computed tomography (CT) is Filtered Back Projection (FBP)[8], which is widely used due to its speed and efficiency when a sufficient number of projections is available. In case of a limited number of projections or high noise levels, alternatives include iterative reconstruction methods, for example, Simultaneous Iterative Reconstruction Technique (SIRT)[1], at the expense of increased computational complexity. Iterative methods also allow for the incorporation of various regularization techniques to improve reconstruction quality. Common choices include Tikhonov regularization, which promotes overall smoothness, and total variation (TV) regularization, which encourages piecewise smoothness by preserving edges while reducing noise.

A common approach to representing the reconstructed volume is by discretizing it into a regular grid of voxels, where each voxel represents a small cubic volume element with a uniform attenuation value. The reconstruction process then involves estimating the attenuation value for each voxel such that the projections of these estimated values align as closely as possible with the measured projection data. This method transforms the continuous problem of reconstructing a continuous attenuation field into a discrete optimization problem, where the goal is to find a set of voxel values that best explain the available projection measurements.

Recently, neural fields have emerged as a powerful tool for representing continuous functions[21], with notable success in applications such as novel-view synthesis of radiance fields, where they have achieved high-fidelity results [15]. Since novel-view synthesis shares some similarities with tomographic reconstruction, neural fields have also been explored for use in tomography. Several studies have applied neural fields to tomography, including CoIL [22], IntraTomo[23], NeAT[18], NAF[25], Angiography NeRF and [14] and SAX [4]. Additionally, advancements in radiance field representation, such as Gaussian splitting, have been investigated in the context of tomographic reconstruction [24], [3], showing promise for improving reconstruction quality in these applications.

One of the great advantages of using neural fields for representing the reconstructed volume lies in the flexibility gained to supplement the loss functions with additional terms. For example, in [10], the authors propose a method to regularize the reconstruction by adding a term similar to total variation.

However, while adding regularization can improve reconstruction quality, determining the nature and strength of the regularization terms remains a challenging task. In this work, we address this issue by proposing the use of data-driven adversarial learning as a regularization technique for tomographic reconstruction. This approach enables the model to learn from existing high-quality data and apply that knowledge to guide the reconstruction process.

Adversarial learning has proven effective in a wide range of tasks, most notably in Generative Adversarial Networks (GANs) [6] for image generation. In the context of tomographic reconstruction, adversarial techniques have been explored in works like [16] and [13], but these approaches have not yet been combined with neural fields, which is the focus of our proposed method.

In addition to adversarial learning, other approaches have been explored for tomographic reconstruction from sparse views. These include methods using convolutional neural networks [9], [26], as well as neural fields [11], [12]. Moreover, a range of related challenges have been tackled in the field, such as Doppler tomography [7], refractive view tomography [27], and sparse view regularization [2], alongside broader topics like CT understanding and diagnostics [5].

2 Method

We propose a novel approach to tomographic reconstruction that combines continuous neural field representations with an adversarial training framework. The key innovation of our method lies in the integration of an adversarial loss, which introduces structural prior knowledge into the reconstruction process. This loss improves the realism and consistency of the reconstructed attenuation fields, leading to more accurate and high-quality volumetric reconstructions from sparse and noisy projection data.

For the adversarial loss, our method uses a training set of volumes that share similar characteristics to the volume we are trying to reconstruct. This training set can consist of volumes reconstructed from data with less noise or more projections, providing a rich source of prior information. The core problem

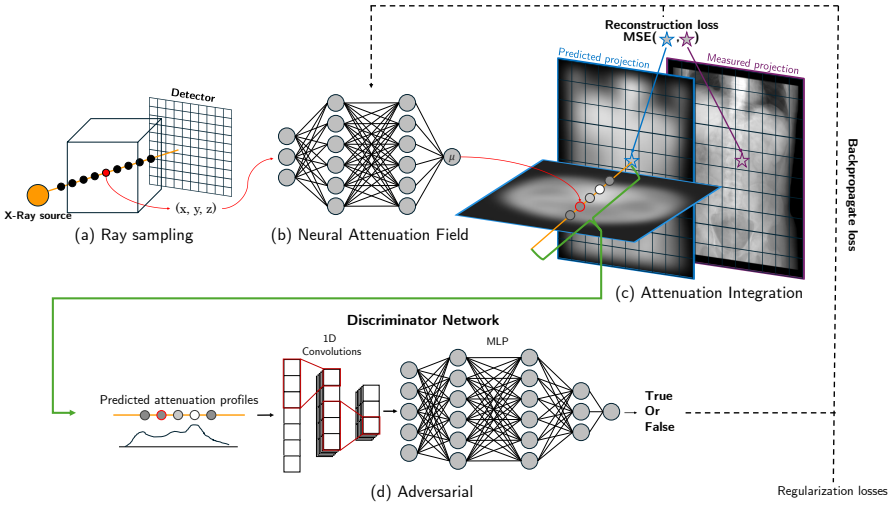

Fig. 1: Illustration of AI-NF training pipeline. (a) Point coordinates are sampled along the ray path extending from the source to the detector. (b) The neural field processes these points and returns predicted attenuation coefficients, yielding the attenuation profile along the ray path. (c) To obtain the predicted value for the detector pixel, the attenuation profile is integrated. This predicted value is compared to the target value from the measured projection, resulting in the reconstruction loss. (d) The attenuation profile is also passed through a discriminator network. This network consists of a 1D convolutional feature extractor followed by an MLP, which predicts whether the attenuation profile originates from a distribution of real attenuation profiles or is generated by the neural field. This prediction yields the adversarial loss based on binary cross entropy. The reconstruction loss, adversarial loss, and additional regularization losses are back-propagated to update the neural field. Although the training of the discriminator is not depicted in the figure, the discriminator network is trained simultaneously with the neural field by providing it with real attenuation profiles from previous high-resolution reconstructions in addition to the predicted attenuation profiles.

we address is the reconstruction of a previously unseen volume, which, while similar to those in the training set, is derived from a sparse and noisy set of projections. By leveraging the structural patterns learned from the training set, our method can better handle the challenges posed by incomplete or low-quality data.

The reconstruction process in our method is formulated for a single ray connecting the X-ray source to a pixel on the projection image. During reconstruction, we iterate over rays. This formulation allows our approach to be flexible and applicable to a wide variety of geometric imaging configurations, including parallel beam, cone beam, and plenoptic imaging. By working in this ray-based framework, we maintain generality across different types of tomographic setups, ensuring that our method can be used in diverse imaging scenarios without requiring significant changes to the underlying model.

2.1 Neural Attenuation Field

The neural attenuation field is a neural network-based model that maps continuous 3D coordinates $\mathbf{x} \in \mathbb{R}^3$ to local attenuation coefficients $\mu(\mathbf{x}) \in [0, 1]$. This mapping is realized through a parameterized neural network that takes the input coordinates and processes them to predict the corresponding attenuation at that point in space. Specifically, we use hash encoding and a multilayer perceptron (MLP) architecture with a skip connection to perform this mapping.

Our neural attenuation field is strongly influenced by [15] and almost identical to [25] in structure. Unlike radiance fields modeled in [15], the attenuation field is view-independent and scalar-valued, so our field has 3D input and 1D output.

Hash encoding. The first step involves passing the 3D coordinates through a multiresolution hash encoding function $\phi(\cdot)$, which captures multi-scale features of the input coordinates and allows for efficient representation of high-dimensional spatial data

$$\mathbf{h} = \phi(\mathbf{x}).$$

Here, $\phi(\cdot)$ aggregates features from multiple resolution levels with a subsequent ReLU activation. This step is motivated by [17] and the use of hash encoding in [25].

MLP. An MLP, denoted $f(\cdot)$, processes the encoded coordinate $\mathbf{h}$ to predict the attenuation coefficient

$$\mu(\mathbf{x}) = f(\mathbf{h}).$$

The MLP network consists of six fully connected layers. Each of the first five layers contains 256 neurons with ReLU activations. The final layer has a single neuron followed by a sigmoid activation to ensure the output is within the desired range. Additionally, a skip connection merges the network input with the activation from the third layer.

2.2 Forward Projection

To optimize the neural attenuation field, we need to produce predicted projections of the field, simulating the process of obtaining projection data. For this, we integrate the continuous attenuation field along a ray and repeat this for every pixel of projection data.

Consider a ray with a known start (X-ray source) and endpoint (the detector pixel) with the length L. We discretize the ray into N equidistant sample points $\{\mathbf{x}_1, \ldots, \mathbf{x}_N\}$, with predicted attenuation coefficients $\{\mu_1, \ldots, \mu_N\}$. The spacing between points is

$$dx = \frac{L}{N}$$

and the predicted projection value for the ray is approximated by

$$\hat{p} = \sum_{i=1}^{N} \mu_i \, dx.$$

2.3 Reconstruction Loss and Model-Based Regularization

Our training objective comprises several loss components, designed to ensure accurate reconstruction while imposing regularization and structural consistency through adversarial supervision.

Reconstruction Loss. The primary loss is the mean squared error (MSE) between the predicted projection $\hat{p}$ and the measured projection p:

$$L_{\text{recon}} = \frac{1}{M} \sum_{j=1}^{M} \left(\hat{p}^{(j)} - p^{(j)} \right)^2,$$

where M is the number of measured rays.

Model-based Regularization. All model-based regularization contributions are formulated per one projection ray.

(a) Smoothness loss is used to promote spatial continuity along each ray

$$L_{\text{smooth}} = \lambda_{\text{smooth}} \frac{1}{N-1} \sum_{i=1}^{N-1} \left| \mu_{i+1} - \mu_i \right|.$$

(b) Consistency loss enforces the stability of the attenuation field by perturbing the input coordinates with a small noise ϵ

$$L_{\text{cons}} = \lambda_{\text{cons}} \frac{1}{N} \sum_{i=1}^{N} \left(\mu(\mathbf{x}_i) - \mu(\mathbf{x}_i + \epsilon) \right)^2.$$

(c) Curvature loss discourages abrupt transitions in the attenuation field, by penalizing the second finite difference

$$L_{\text{curv}} = \lambda_{\text{curv}} \frac{1}{N-2} \sum_{i=2}^{N-1} |\mu_{i-1} - 2\mu_i + \mu_{i+1}| \,.$$

2.4 Adversarial Loss and Feature Matching

Our key contribution is the integration of an adversarial loss that injects structural prior knowledge into the reconstruction. As with model-based regularization, the adversarial loss and feature matching are formulated per one projection ray. This is important, as it is easy to incorporate in any reconstruction model.

(a) **Adversarial Loss:** We train a discriminator D to distinguish between ray profiles originating from the training data (*real* rays), and the profiles originating from the neural attenuation field (*fake* rays). We then train the generator to produce outputs that the discriminator classifies as *real*

$$L_{\text{adv}} = \lambda_{\text{adv}} \cdot \mathbb{E}\left[-\log\left(D(\mu(\mathbf{x}))\right)\right] .$$

(b) **Feature Matching Loss:** To further guide the generator, we minimize the difference between intermediate features extracted from *real* and *fake* rays

$$L_{\text{fm}} = \lambda_{\text{fm}} \cdot \|\mathbf{f}_{\text{real}} - \mathbf{f}_{\text{fake}}\|_2^2 \,.$$

Total Generator Loss We gradually increased the influence of the data-driven terms during training using a sigmoid ramp-up function

$$\gamma = \frac{1}{1 + \exp\left(-\kappa\left(t_{\text{epoch}} - t_{\text{midpoint}}\right)\right)} .$$

The overall loss for the generator is then defined as

$$L_G = L_{\text{recon}} + L_{\text{smooth}} + L_{\text{cons}} + L_{\text{curv}} + \gamma\left(L_{\text{adv}} + L_{\text{fm}}\right) .$$

2.5 Discriminator Network

The discriminator is designed to enforce structural realism by providing feedback to the generator.

Convolutional Pipeline The attenuation profile of a ray, represented as a 1D tensor $\mathbf{r} \in \mathbb{R}^N$, is reshaped to $(1, N)$ and processed through a series of convolutional layers with spectral normalization. Early layers use larger kernels (e.g., kernel size 7 with stride 2) to capture coarse features, while subsequent layers refine the representation with smaller kernels.

Self-Attention Module A self-attention block is applied to the convolutional features to capture long-range dependencies. Given feature maps $x \in \mathbb{R}^{B\times C\times L}$, we compute:

$$Q = W_q * x, \quad K = W_k * x, \quad V = W_v * x,$$

where W_q, W_k, and W_v are learned convolutional filters. The attention map is then:

$$A = \text{softmax}(Q^\top K),$$

and the output of the self-attention module is:

$$\text{Out} = \gamma_{\text{attn}} \cdot (VA^\top) + x,$$

with γ_{attn} as a learnable scaling parameter.

Feature Aggregation and Classification Global average pooling is applied to the self-attention enhanced features to obtain a base feature $\mathbf{f}_{\text{base}}$. This base feature is concatenated with the ray's start and end coordinates, $\mathbf{s}, \mathbf{e} \in \mathbb{R}^3$, to form:

$$\mathbf{f}_{\text{input}} = \text{concat}(\mathbf{f}_{\text{base}}, \mathbf{s}, \mathbf{e}).$$

A final MLP processes $\mathbf{f}_{\text{input}}$ and outputs a scalar validity score:

$$D(\mathbf{r}, \mathbf{s}, \mathbf{e}) = \sigma\left(f_{\text{MLP}}(\mathbf{f}_{\text{input}})\right),$$

where σ denotes the sigmoid activation function.

The discriminator is trained using binary cross-entropy loss to distinguish between *real* profiles and the *fake* profiles generated by the network.

2.6 Training Procedure

Training is conducted in an alternating fashion between the generator and the discriminator.

- **Generator Update:** The generator is updated by minimizing the composite loss L_G, which includes reconstruction, regularization, and gradually introduced adversarial terms.
- **Discriminator Update:** The discriminator is updated to improve its ability to distinguish *real* from *fake* ray profiles using binary cross-entropy loss.

Both networks are optimized using separate AdamW optimizers. The adversarial component is progressively ramped up to allow the generator to first establish accurate reconstructions before incorporating structural priors through adversarial feedback.

During training, the network is fed sequences of points along ray paths; the reconstruction loss is computed only for rays with measured detector values, while extra rays - generated from supplementary positional data — expand the range of ray paths used in both the adversarial and regularization losses. Corresponding *real* ray profiles (including start and end coordinates) are provided

for both measured and extra rays and are used solely for the adversarial loss, which enforces structural priors and guides the network toward more realistic reconstructions.

The final result, CT reconstruction, is obtained by sampling generator on the regular grid of the reconstruction domain.

3 Experiments

Experiments were conducted on volumes from the Task07_Pancreas dataset from the Medical Segmentation Decathlon [20]. Reconstructions were performed on the central slice using 16 evenly spaced projections spanning 0–180°, under both ideal conditions (without sinogram noise) and with a noise level of 2% on the sinogram. For adversarial training, two ray profile datasets were constructed from 100 volumes: one using the same 16 projection angles as for reconstruction, and another using 200 evenly spaced angles also over 0–180°.

Four methods were compared: FBP, SIRT, an implementation of a neural field without adversarial loss (similar to NAF), and our proposed method adversarially informed neural field (AI-NF).

To evaluate the quality of the reconstruction we compare the ground truth volume noise-free against the reconstructed volume using MSE (mean squared error) PSNR (peak signal to noise ratio, and SSIM (structural similarity index measure). Furthermore, we report the MSE for the predicted projections compared to the available sinogram data, i.e. noisy data in case of experiments with noise.

The model was trained using the following hyperparameters: the number of points sampled per ray was set to 512. Both models were trained using the AdamW optimizer from PyTorch, with the neural field having a learning rate of 1×10^{-3} and the discriminator having a learning rate of 1×10^{-4}. The training was conducted for 1000 epochs, with a batch size of 3500 for rays with known projection values, and an additional 1500 rays with no known projection value. The regularization weights were set as follows: adversarial weight $\lambda_{\text{adv}} = 1{\times}10^{-3}$, smoothness weight $\lambda_{\text{smooth}} = 5 \times 10^{-5}$, curvature weight $\lambda_{\text{curv}} = 1 \times 10^{-5}$, consistency weight $\lambda_{\text{cons}} = 5{\times}10^{-2}$, and feature matching weight $\lambda_{\text{fm}} = 1{\times}10^{-3}$. For the sigmoid ramp-up, the midpoint parameter t_{midpoint} was set to 0.15, and the sharpness parameter κ was set to 0.05.

4 Results

Under noise-free conditions, our approach yields quantitative performance that is comparable to, and in some cases slightly superior to, SIRT in terms of both mean squared error (MSE) and peak signal-to-noise ratio (PSNR) in the reconstruction. However, when reconstructing from a noisy sinogram, our adversarially informed neural field (AI-NF) method demonstrates a noticeable improvement over both SIRT and the baseline neural field (NF) without adversarial loss (see Table 1). Specifically, while the addition of noise leads to a PSNR reduction

of 2.44 dB and an SSIM decrease of 0.32 for SIRT, the AI-NF method only exhibits a minor PSNR decline of 0.57 dB and a negligible change in SSIM (+0.01). This indicates that the incorporation of adversarial regularization significantly enhances the robustness of the reconstruction in the presence of noise.

Figure 2 presents a qualitative comparison of the reconstructions obtained by various methods using both clean and noisy sinograms. The results clearly demonstrate that the AI-NF method maintains high fidelity under noise, with its reconstruction from noisy data closely resembling that from the clean sinogram. In contrast, the SIRT reconstruction exhibits noticeable stripe-like artifacts in the presence of noise.

Additionally, Figure 3 illustrate the predicted sinograms, the measured sinograms, and their corresponding residuals across different methods. As expected, the FBP method performs poorly due to the limited number of projections. In contrast, SIRT, NF, and AI-NF all perform reasonably well. Though some edge effects can be seen in the residual of the AI-NF sinogram.

Dataset	**Model**	**Reconst. MSE ↓**	**Reconst. PSNR ↑**	**Reconst. SSIM ↑**	**Project. MSE ↓**
Pancreas 16	FBP	0.0450	13.46	0.395	0.0970
	SIRT	0.0032	24.97	**0.747**	2e-4
	Neural Field	0.0035	24.52	0.738	**2.5e-5**
	AI-NF (ours)	**0.0030**	**25.24**	0.715	5.26e-5
Pancreas 16 with noise	FBP	0.0438	13.59	0.393	0.0974
	SIRT	0.0056	22.53	0.428	5e-4
	Neural Field	0.0063	21.99	0.582	4e-4
	AI-NF (ours)	**0.0034**	**24.68**	**0.724**	**2e-4**

Table 1: MSE, PSNR and SSIM measurements on reconstructed volume and MSE measurements on projections, for four methods on noise free and noisy sinograms.

5 Conclusion

We have presented an adversarially informed neural field (AI-NF) method for tomographic reconstruction that demonstrates superior robustness to sinogram noise compared to traditional iterative methods such as SIRT. Under noisy conditions, our approach effectively mitigates artifacts and preserves reconstruction fidelity, while reconstructions from clean sinograms remain competitive with established techniques.

Under ideal (noise-free) conditions, AI-NF performs comparably to SIRT, albeit with increased reconstruction time and a greater need for hyperparameter tuning. These limitations suggest that the advantages of our method are most pronounced in challenging, noise-prone environments where conventional methods struggle.

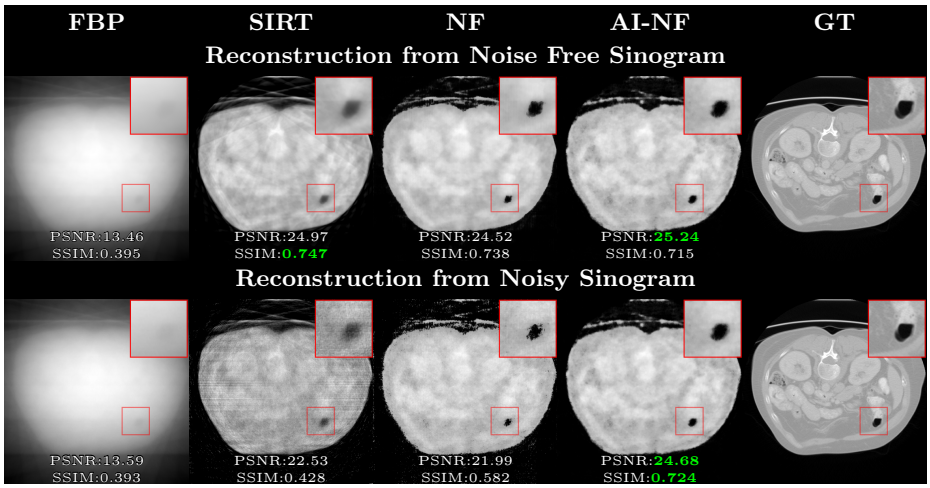

Fig. 2: Qualitative results of reconstruction by four different methods from noise free and noisy sinograms, reconstructions were done from 16 projections. From left to right FBP, SIRT, Neural Field, Adversarially informed Neural Field, and Ground truth.

Future work will explore the impact of incorporating a larger number of volumes in the adversarial loss, as well as investigating whether pre-training the discriminator on extensive datasets can further improve the quality of the learned structural priors. Additionally, optimizing the computational efficiency of the method and refining hyperparameter selection strategies are important directions to ensure broader applicability in clinical and industrial settings.

Overall, our results indicate that integrating adversarial regularization into neural field representations offers a promising path for enhancing tomographic reconstruction, particularly in scenarios where projection data is sparse or contaminated by noise.

References

1. Andersen, A.H., Kak, A.C.: Simultaneous algebraic reconstruction technique (SART): a superior implementation of the art algorithm. Ultrasonic imaging **6**(1), 81–94 (1984)
2. Ayad, I., Larue, N., Nguyen, M.K.: QN-mixer: A quasi-Newton MLP-mixer model for sparse-view CT reconstruction. In: Proceedings of the IEEE/CVF Conference on Computer Vision and Pattern Recognition. pp. 25317–25326 (2024)
3. Cai, Y., Liang, Y., Wang, J., Wang, A., Zhang, Y., Yang, X., Zhou, Z., Yuille, A.: Radiative Gaussian splatting for efficient X-ray novel view synthesis. In: European Conference on Computer Vision. pp. 283–299. Springer (2025)

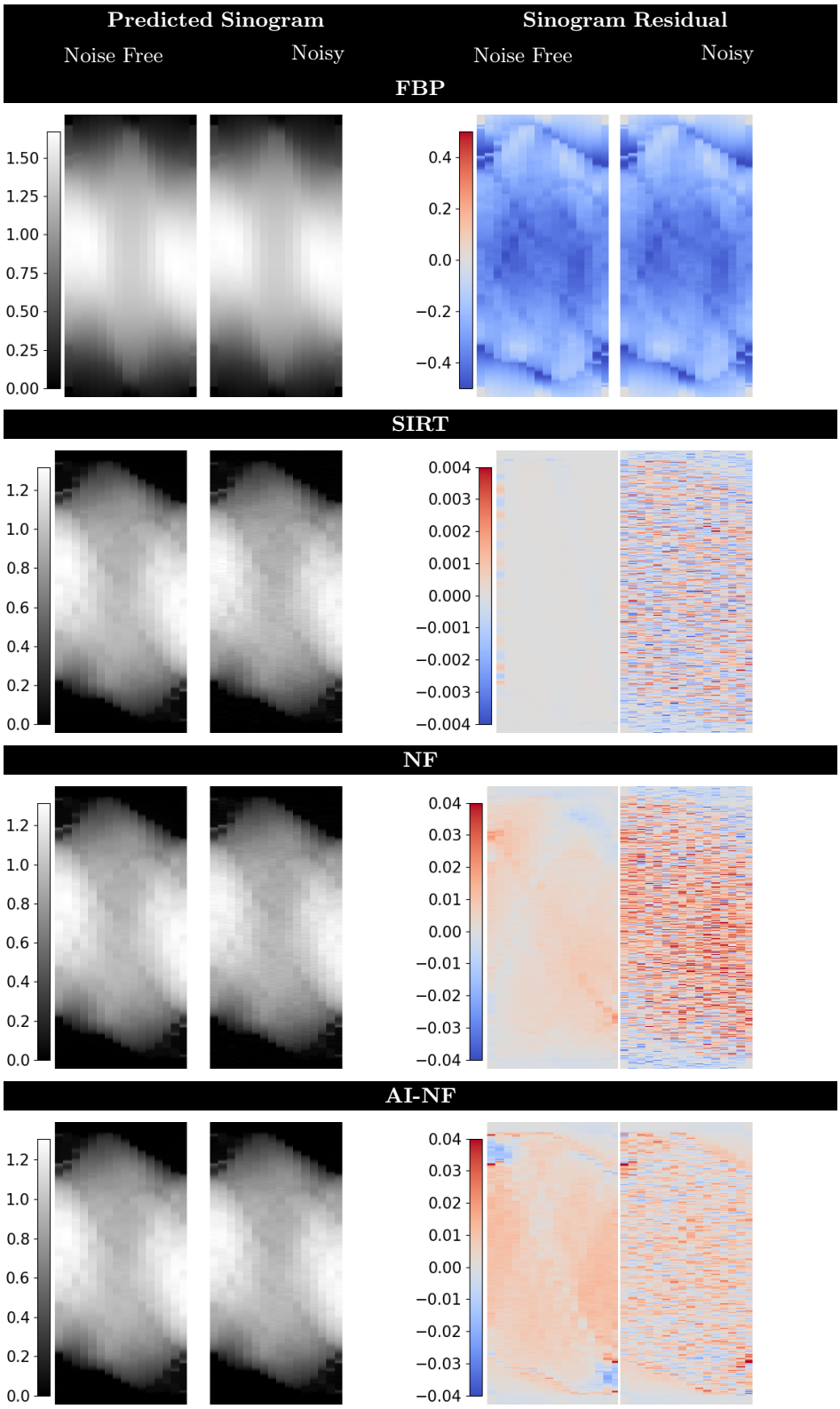

Fig. 3: Predicted sinogram when reconstructing from noise-free and noisy sinograms

4. Cai, Y., Wang, J., Yuille, A., Zhou, Z., Wang, A.: Structure-aware sparse-view X-ray 3D reconstruction. In: Proceedings of the IEEE/CVF Conference on Computer Vision and Pattern Recognition. pp. 11174–11183 (2024)
5. Cao, W., Zhang, J., Xia, Y., Mok, T.C., Li, Z., Ye, X., Lu, L., Zheng, J., Tang, Y., Zhang, L.: Bootstrapping chest CT image understanding by distilling knowledge from X-ray expert models. In: Proceedings of the IEEE/CVF Conference on Computer Vision and Pattern Recognition. pp. 11238–11247 (2024)
6. Goodfellow, I., Pouget-Abadie, J., Mirza, M., Xu, B., Warde-Farley, D., Ozair, S., Courville, A., Bengio, Y.: Generative adversarial networks. Communications of the ACM **63**(11), 139–144 (2020)
7. Huang, T., Miller, J., Prabhakara, A., Jin, T., Laroia, T., Kolter, Z., Rowe, A.: DART: Implicit doppler tomography for radar novel view synthesis. In: Proceedings of the IEEE/CVF Conference on Computer Vision and Pattern Recognition. pp. 24118–24129 (2024)
8. Kak, A.C., Slaney, M.: Principles of computerized tomographic imaging. SIAM (2001)
9. Kasten, Y., Doktofsky, D., Kovler, I.: End-to-end convolutional neural network for 3D reconstruction of knee bones from bi-planar X-ray images. In: Machine Learning for Medical Image Reconstruction: Third International Workshop, MLMIR 2020, Held in Conjunction with MICCAI 2020, Lima, Peru, October 8, 2020, Proceedings 3. pp. 123–133. Springer (2020)
10. Koo, J., Brenne, E.O., Dahl, A.B., Dahl, V.A.: A tomographic reconstruction method using coordinate-based neural network with spatial regularization. In: Northern Lights Deep Learning Workshop 2021. Presses Universitaires du Septentrion (2021)
11. Lin, Y., Luo, Z., Zhao, W., Li, X.: Learning deep intensity field for extremely sparse-view CBCT reconstruction. In: International Conference on Medical Image Computing and Computer-Assisted Intervention. pp. 13–23. Springer (2023)
12. Lin, Y., Yang, J., Wang, H., Ding, X., Zhao, W., Li, X.: C^2RV: Cross-regional and cross-view learning for sparse-view CBCT reconstruction. In: Proceedings of the IEEE/CVF Conference on Computer Vision and Pattern Recognition (CVPR). pp. 11205–11214 (June 2024)
13. Lunz, S., Öktem, O., Schönlieb, C.B.: Adversarial regularizers in inverse problems. Advances in neural information processing systems **31** (2018)
14. Maas, K.W., Pezzotti, N., Vermeer, A.J., Ruijters, D., Vilanova, A.: NeRF for 3D reconstruction from X-ray angiography: Possibilities and limitations. In: VCBM 2023: Eurographics Workshop on Visual Computing for Biology and Medicine. pp. 29–40. Eurographics Association (2023)
15. Mildenhall, B., Srinivasan, P.P., Tancik, M., Barron, J.T., Ramamoorthi, R., Ng, R.: NeRF: Representing scenes as neural radiance fields for view synthesis. Communications of the ACM **65**(1), 99–106 (2021)
16. Mukherjee, S., Öktem, O., Schönlieb, C.B.: Adversarially learned iterative reconstruction for imaging inverse problems. In: International Conference on Scale Space and Variational Methods in Computer Vision. pp. 540–552. Springer (2021)
17. Müller, T., Evans, A., Schied, C., Keller, A.: Instant neural graphics primitives with a multiresolution hash encoding. ACM Trans. Graph. **41**(4), 102:1–102:15 (Jul 2022). https://doi.org/10.1145/3528223.3530127, https://doi.org/10.1145/3528223.3530127
18. Rückert, D., Wang, Y., Li, R., Idoughi, R., Heidrich, W.: NeAT: Neural adaptive tomography. ACM Transactions on Graphics (TOG) **41**(4), 1–13 (2022)

19. Shin, H., Kim, T., Lee, J., Chun, S.Y., Cho, S., Shin, D.: Sparse-view cbct reconstruction using meta-learned neural attenuation field and hash-encoding regularization. Computers in Biology and Medicine **189**, 109900 (2025). https://doi.org/https://doi.org/10.1016/j.compbiomed.2025.109900, https://www.sciencedirect.com/science/article/pii/S0010482525002513
20. Simpson, A.L., Antonelli, M., Bakas, S., Bilello, M., Farahani, K., van Ginneken, B., Kopp-Schneider, A., Landman, B.A., Litjens, G., Menze, B.H., Ronneberger, O., Summers, R.M., Bilic, P., Christ, P.F., Do, R.K.G., Gollub, M., Golia-Pernicka, J., Heckers, S., Jarnagin, W.R., McHugo, M., Napel, S., Vorontsov, E., Maier-Hein, L., Cardoso, M.J.: A large annotated medical image dataset for the development and evaluation of segmentation algorithms. CoRR **abs/1902.09063** (2019), http://arxiv.org/abs/1902.09063
21. Sitzmann, V., Martel, J., Bergman, A., Lindell, D., Wetzstein, G.: Implicit neural representations with periodic activation functions. Advances in neural information processing systems **33**, 7462–7473 (2020)
22. Sun, Y., Liu, J., Xie, M., Wohlberg, B., Kamilov, U.S.: CoIL: Coordinate-based internal learning for tomographic imaging. IEEE Transactions on Computational Imaging **7**, 1400–1412 (2021)
23. Zang, G., Idoughi, R., Li, R., Wonka, P., Heidrich, W.: IntraTomo: self-supervised learning-based tomography via sinogram synthesis and prediction. In: Proceedings of the IEEE/CVF International Conference on Computer Vision. pp. 1960–1970 (2021)
24. Zha, R., Lin, T.J., Cai, Y., Cao, J., Zhang, Y., Li, H.: R^2-Gaussian: Rectifying radiative Gaussian splatting for tomographic reconstruction. arXiv preprint arXiv:2405.20693 (2024)
25. Zha, R., Zhang, Y., Li, H.: NAF: neural attenuation fields for sparse-view cbct reconstruction. In: International Conference on Medical Image Computing and Computer-Assisted Intervention. pp. 442–452. Springer (2022)
26. Zhang, Y., Yao, Z., Klöfkorn, R., Ritschel, T., Villanueva-Perez, P.: 4D-ONIX: A deep learning approach for reconstructing 3D movies from sparse X-ray projections. arXiv preprint arXiv:2401.09508 (2024)
27. Zhao, B., Levis, A., Connor, L., Srinivasan, P.P., Bouman, K.L.: Single view refractive index tomography with neural fields. In: Proceedings of the IEEE/CVF Conference on Computer Vision and Pattern Recognition. pp. 25358–25367 (2024)